

AperTO - Archivio Istituzionale Open Access dell'Università di Torino

Chitosan crosslinked flat scaffolds for peripheral nerve regeneration

This is the author's manuscript

Original Citation:

Availability:

This version is available <http://hdl.handle.net/2318/1625674> since 2017-02-24T11:28:18Z

Published version:

DOI:10.1088/1748-6041/11/4/045010

Terms of use:

Open Access

Anyone can freely access the full text of works made available as "Open Access". Works made available under a Creative Commons license can be used according to the terms and conditions of said license. Use of all other works requires consent of the right holder (author or publisher) if not exempted from copyright protection by the applicable law.

(Article begins on next page)

Chitosan Crosslinked Flat Scaffolds for Peripheral Nerve Regeneration

F. Fajana¹, B. Cigdem², S. Tao¹, A. Gama¹, G. Chakrab¹, E. Rana¹, C. Tada Tsui¹, S. Ghose¹, S. Kulkarni¹

¹Department of Chemical and Biological Sciences and Center for High Performance Polymers, University of Texas, Roper Center, 3038M1, Odessa, TX

²Department of Chemistry, Oklahoma Department, Trauma Center Hospital (OTC), 160 West 20, 74108, Tulsa, Oklahoma

³Department of Mechanical and Aerospace Engineering, Politecnico di Torino, Corso Duca degli Abruzzi 24, 10129, Torino, Italy

Presented at:
⁴Department of Polymer Science, University of Texas, Large Research 2, 30001, Odessa, TX, USA

Corresponding author:
Sudipta Kulkarni
Department of Chemical and Biological Sciences, University of Texas,
Roper Center 30
3038M1 Odessa, TX
Tel: +1(409) 325-5121, fax: +1(409) 325-5120
E-mail: sudipta.kulkarni@utexas.edu

Abstract

Chitosan (CS) has been widely used in a variety of biomedical applications, including peripheral nerve repair. Due to its excellent biocompatibility, biodegradability, stability, availability, and antifouling activity, in this study, CS hydrogels crosslinked with chitosan sulfonic polyacrylate (SDSP) alone (CS/SDSP) or in combination with γ-poly(D-glutamic acid)/methacrylate chitosan (CS/GPTMS/SDSP) were fabricated with a wet-spin casting technique. The crosslinking ratio of crosslinking agent and CS was precisely adjusted to obtain a composite material having both adequate mechanical properties and high biocompatibility. In vitro cytotoxicity tests showed that both CS hydrogels allowed cell survival and proliferation. Moreover, CS/GPTMS/SDSP membranes promoted cell adhesion, induced Schwann cell-like morphology and supported neurite outgrowth both in vitro and in vivo. Preliminary in vivo tests carried out on both types of nerve scaffolds (CS/SDSP and CS/GPTMS/SDSP membranes) demonstrated that provided for: (i) promoting, as a membrane, the rate of nerve conduction repair by end-to-end surgery and avoiding post-operative nerve adhesion; (ii) helping, as a scaffold, the two nerve segments after a nerve peripheral nerve lesion with reference time. A long-term rat median nerve was repaired using CS/SDSP and CS/GPTMS/SDSP conduits to further investigate their ability to induce nerve regeneration in vivo. CS/GPTMS/SDSP tubes revealed to be more highly biocompatible and, using a 12-week post-operative layer of time, they showed from the distal nerve repair. On the contrary, CS/SDSP conduits presented more than 60% regeneration and functional recovery leading to an outcome comparable to median nerve repaired by autograft.

Key words: Polyphased nerve repair, regeneration, fibrillation, chronic Schwann cells.

1. Introduction

Polyphased nerve transection due to car accidents, sport and military injuries [1] are reported to affect, annually, more than one million people worldwide.

The possibility to repair nerve function is dependent on the severity of the damage sustained. Spontaneous recovery is possible only if the continuity of the nerve is maintained. In case of complete nerve transection, a suture is required for re-establishing a continuity between the proximal and the distal stumps. Autologous nerve grafts (anastomosis) is the "gold standard" technique for repairing peripheral nerve defects and is essential in the case of healthy nerve. Regrowth of sensory origin centrally the axonal nerve (for holding the grip) [2].

However, the practice presents some disadvantages: it requires an additional incision for harvesting the healthy sensory nerve, leading to a sensory deficit, yet, graft material is limited especially in case of an extended nerve lesion. In an alternative, a variety of biomaterials for nerve reconstruction has been developed [3-6]. In particular, chitosan (CS), as a natural polysaccharide, has recently attracted more and more attention due to its good biocompatibility, biodegradability, non-toxicity, ready availability and easy physicochemical properties [3-6].

Recent in vitro studies revealed the suitability of CS membranes as substrate for survival and neuronal Schwann cell (SC) growth [7] as well as survival and differentiation of neuronal cells [8, 9].

CS-based biodegradable scaffolds have been widely used for neural repair in different animal models [10]. CS-based nerve conduits, alone or in combination with other biomaterials, have been found to bridge effectively peripheral nerve defects [11-13]. In CS nerve guides applied with the introduction of a biophysical CS membrane were used to reconstruct 10 mm sciatic nerve defects in adult healthy and diabetic rats, demonstrating an enhancement in functional and morphological nerve regeneration [14].

Standard nerve regeneration of long gaps has also been reported when CS cables are coated with poly(urea and polyurethane) or polyurethane and polyurethane and polyurethane (13,14). Functionalized poly(urethane) (15) Because poly(urea and polyurethane) (13,14), improved techniques and different crosslinking methods have been developed to increase the poor mechanical strength of CS nerve guide channel under physiological conditions, which is one of the main factors limiting the CS nerve to clinical application for neurological and non (16).

In the present work, ethane sulfonic phosphate (ESP) and poly(ethylene glycol) dimethyl ether (PEG) modified CS for membrane, previously characterized in terms of physicochemical, thermal, morphological, mechanical properties (16), were evaluated in terms of biological properties using in vitro and in vivo tests.

In vitro studies on R15 DMPT with were performed on adaptable CS based flat membranes to evaluate biocompatibility and to assess their potential applicability as nerve repair conduits. In addition, CS flat membranes and conduits were tested *in vivo* in the model of rat median nerve repair. The outcome of nerve reconstruction was assessed at 12 weeks postimplantation through a combination of functional assessment, histological and morphological investigation.

2. Methods

2.1 Membrane preparation

CS membrane substrate weight 70%-80% divinylbenzene degree, Sigma Aldrich) was dissolved in acetic acid solution 0.5M at room temperature by continuous stirring to obtain a 2.5 % (w/v) solution. Crosslinked membranes were prepared according to the method previously described by Rami and colleagues [20]. Briefly:

1. DSP-entrained samples (CS/DSP) were obtained by adding DSP (10 mm drop per second) to the CS solution with a concentration of 7.5 % w/v with respect to the actual polymer solution volume. The mixed solution was kept under stirring at room temperature for about 10 minutes.

2. CS/DSP/DSP-entrained samples (CS/GPTMS)_DSP were obtained adding GPTMS (0.5% w/v) to the CS solution. The resulting CS/GPTMS solution was kept under stirring for 1 hour followed by the dispersive addition (one drop per second) of DSP (10 concentration 7.5 % w/v) and maintained under continuous stirring for 10 minutes.

Finally, 10 mL of each solution (CS/DSP and CS/GPTMS)_DSP) were poured into a cast Petri dishes and co-dried for 48 h to obtain flat membranes. All crosslinked disk samples were dipped into demineralized water for 10 minutes and then the water pH values were measured to evaluate the presence of acidic residues.

Finally wet were performed by the authors, on CS/DSP and CS/GPTMS)_DSP membranes, both in dry and in wet conditions [20].

2.2 In vitro cell tests on CS based membranes

In vitro cell tests were performed using BHK-212FTE, a heterotetraploid cell line (ATCC - catalog number CRL-2730). Cytotoxicity tests were carried out on both CS/DSP and CS/GPTMS)_DSP while, MTT-DHBT adhesion, proliferation and gene expression were evaluated on CS/GPTMS)_DSP due to the

higher mechanical stability of the filament under physiological conditions and because they were considered as "the most pure" membranes required for CS/GPDM, DSP fabrication were the case of CS/DSP supplemented with GPDM). Visible elongation of dried non-porous DMG cultured on CS/GPDM, DSP was determined by confocal laser microscopy.

3.2.1 Cytotoxicity study on CS/GPDM, DSP and CS/DSP

The effect of the CS based material extracts was studied as MTT-DMSO, CS/DSP and CS/GPDM, DSP samples were incubated with a 20 minutes exposure to ultraviolet (UV) irradiation (UV lamp wavelength 254 nm, UltravioletSource, Co., St. Louis, MO). Appropriate control extracts were prepared by incubating both sterilized CS based membranes in Dulbecco's Modified Eagle Medium (DMEM, Sigma Aldrich) supplemented with 100 IU/ml penicillin (Sigma), 0.1 mg/ml streptomycin (Sigma), 5 mM sodium pyruvate (Sigma), 4 mM L-glutamine (Sigma) and 10% heat-inactivated fetal bovine serum (FBS, Gibco Technologies) and stored at 37 °C in a humidified atmosphere of 5% CO₂ for 15 days. As control media, samples of culture medium were incubated in the same conditions of CS/DSP and CS/GPDM, DSP samples and then collected after 15 days. These pre-conditions were used for cell line pre-culture on empty cultured media. In detail, MTT-DMSO cells were seeded and cultured in the previous prepared control media, at a density of 2x10⁴ cells/ml on 96-well dishes. After 2, 5, 7 and 7 days in vitro (DIV) cells were trypsinized and counted in a Beckman's beta-scintillation counter. Experiments were performed on technical replicates. The counts obtained from average were analyzed, averaged and expressed in logarithmic scale of viable cells/cm² x 10³.

3.2.2 Cell adhesion on CS/GPDM, DSP membranes

Immunocytochemistry analysis was performed on quadruplicate culture cell adherent and morphology. K562-DSP7 were washed at a density of 1×10^5 cells/ml in methanol and stained glass slides. After 24 hours of culture, culture medium was removed, substrates with attached cells were rinsed with PBS and fixed by the addition of 4% paraformaldehyde solution (PFA, Sigma-Aldrich). After 20 min the PFA was removed and each plate was washed with PBS. Fixed cells were permeabilized with 0.1% Triton X-100 and blocked with 1% Normal goat serum in 0.05M PBS (pH 7.4) for 1 h at room temperature. F-actin was detected using TRITC-conjugated phalloidin (Fluorolab) in blocking solution (Chemicon/Millipore) by 1 h incubation at room temperature. Following three wash steps of 5 min each, Vectashift was detected by overnight incubation with rhodamine microtubule antibody (Mab5p12) (Abcam) diluted 1:200 in PBS followed by 1 h incubation with goat anti mouse Alexa 488 secondary antibody (Invitrogen) diluted 1:200 in PBS.

A quantitative evaluation of the morphology of the cells plated on different substrates was conducted, taking into account the diameter and aspect of filopodia. The value of diameter of tubulated cells was expressed as a percentage of total tubulated cells in each experimental group. All the fluorescently-labeled cells were measured under a LSM 510 confocal laser microscopy system (Zeiss, Axio), which incorporates two beam (argon and HeNe) and is equipped with an inverted Axiovert 100 SB microscope.

3.2.2. Proliferation assay on C567-FIBR-DSP membranes

K562-DSP7 cells were seeded in 96-well plates containing 100 FIBR, at a density of 1.5×10^3 cells/ml in both C567-FIBR-DSP and glass control plates (control). After 1, 3 and 5 days, culture medium was removed, substrates with attached cells were rinsed with PBS and fixed by the addition of 4% PFA. After 20 min, PFA was removed and each plate was washed with PBS. K562-DSP7 cells were stained with 1% crystal violet in deep purple buffer. At the same solution in 200 μ l from substrate (pH 9) for

10 cells of each suspension. Cells were photographed at 200X. Cell counts (microscopy and 10 images) were taken at a time (approximately 10X) for each sample. The images were then acquired through the program Image Manager (IMM) (Leciva). The counts obtained from proliferation assay were analyzed, averaged and expressed as (arithmetic mean \pm standard deviation) \times 10³.

2.2.4 Real Time Reverse Transcriptase Polymerase Chain Reaction (Real Time RT-PCR) analysis via CFX96PAM₉₆qPCR

RNA extraction: Cells were cultured in 200000 cells/ml in 24-well plates. Cells were harvested using RNeasy Lysis Reagent (Qiagen) and total RNA was extracted from the confluent culture by lysis with TRIzol (Invitrogen). The RNA concentration was quantified by measuring the absorbance at 260/280 nm. The total RNA (1 µg per sample) was reverse-transcribed in a reaction volume of 25 µl with 1.5 µM of random hexamers (Thermo Scientific), each reaction contained 1.00U of reverse transcriptase (RT) (BioLabs, Beverly, MA, USA), 75U of RNase H, 10U of RNase H2, 10U of RNase H3, 10U of RNase H4, 10U of RNase H5, 10U of RNase H6, 10U of RNase H7, 10U of RNase H8, 10U of RNase H9, 10U of RNase H10, 10U of RNase H11, 10U of RNase H12, 10U of RNase H13, 10U of RNase H14, 10U of RNase H15, 10U of RNase H16, 10U of RNase H17, 10U of RNase H18, 10U of RNase H19, 10U of RNase H20, 10U of RNase H21, 10U of RNase H22, 10U of RNase H23, 10U of RNase H24, 10U of RNase H25, 10U of RNase H26, 10U of RNase H27, 10U of RNase H28, 10U of RNase H29, 10U of RNase H30, 10U of RNase H31, 10U of RNase H32, 10U of RNase H33, 10U of RNase H34, 10U of RNase H35, 10U of RNase H36, 10U of RNase H37, 10U of RNase H38, 10U of RNase H39, 10U of RNase H40, 10U of RNase H41, 10U of RNase H42, 10U of RNase H43, 10U of RNase H44, 10U of RNase H45, 10U of RNase H46, 10U of RNase H47, 10U of RNase H48, 10U of RNase H49, 10U of RNase H50, 10U of RNase H51, 10U of RNase H52, 10U of RNase H53, 10U of RNase H54, 10U of RNase H55, 10U of RNase H56, 10U of RNase H57, 10U of RNase H58, 10U of RNase H59, 10U of RNase H60, 10U of RNase H61, 10U of RNase H62, 10U of RNase H63, 10U of RNase H64, 10U of RNase H65, 10U of RNase H66, 10U of RNase H67, 10U of RNase H68, 10U of RNase H69, 10U of RNase H70, 10U of RNase H71, 10U of RNase H72, 10U of RNase H73, 10U of RNase H74, 10U of RNase H75, 10U of RNase H76, 10U of RNase H77, 10U of RNase H78, 10U of RNase H79, 10U of RNase H80, 10U of RNase H81, 10U of RNase H82, 10U of RNase H83, 10U of RNase H84, 10U of RNase H85, 10U of RNase H86, 10U of RNase H87, 10U of RNase H88, 10U of RNase H89, 10U of RNase H90, 10U of RNase H91, 10U of RNase H92, 10U of RNase H93, 10U of RNase H94, 10U of RNase H95, 10U of RNase H96, 10U of RNase H97, 10U of RNase H98, 10U of RNase H99, 10U of RNase H100. The reaction mixture was incubated at 42°C for 30 min, 50°C for 30 min and 70°C for 30 min. Specific primers designed to amplify B cell lymphoma 2 (BL2) (accession X protein (BL2)), BCL-2 gene promoter involved in the growth of B-cells, which regulates cellular apoptosis, suppresses apoptosis (BL2), or regulates cellular division in many cell lines, with respect to regulate cell proliferation (BL2) of human cells, a protein encoded by the BL2 gene involved in the regulation of cell growth, cell proliferation, cell death, cell survival, protein synthesis, and transcription are listed below.

BL2 Forward Sequence: TGGCTGGGGCAACTTCAGC; Reverse Sequence:

GAGACCTGGAGACTTGG-362 Forward Sequence- GTAGTACAGCTTGAGT Reverse Sequence- GGCCAGGAGTCCCAAGAG-364 Forward Sequence

GAGGCGCTTATCAGAG- Reverse Sequence- GAGGACAGGGCAAGC- in TMR Forward Sequence- GCTCTTGGCAGGAGGAGGAG- Reverse Sequence-

GCTTWTGAGAGAGAGAGAGAGGAGG- Forward Sequence- CTACAGAGAGAGGTCACAGAG- Reverse Sequence- CCGGACAGCCAGAGAGAG- Reverse Sequence- GGGGAGAGTTTAAAGGCTG-

For identification in multiple sequencing genes, oligonucleotide primers C (180) and 5'3A binding primers (780) were used. The reaction mixture (200 µl) included 7.5 µg dNTPs and 0.1 µM primer.

1.2.5 µM SYBR Green II (Bio-Techne) and 5' of dNTPs. The PCR conditions were as following: initial step at 95°C for 2 min, then 40 cycles at 95°C for 20 s, and 60°C for 1 min. The results were obtained from three independent experiments.

2.2.3. Total protein extraction and western blot

Total proteins were extracted by adding cells in boiling Lysosomal buffer (2% SDS and 0.125 M Tris-HCl pH 6.8, followed by 2 min at 100°C. Protein concentrations were determined by the BCA method, and equal amounts of protein (determined at 100°C in 100 µM 2-mercaptoethanol and 10% glycerol) were loaded into each lane, separated by SDS-PAGE, transferred to a HybondE-CL Extra membrane and blocked for 1 h at 37°C in 1% BSA (1% BSA and 0.5% Triton X-100) and 0.1 M Tris-HCl pH 7.4, and 0.1 M NaCl.

After washing 3 times with 0.05% Triton X-100, membranes were incubated overnight at 4°C in primary antibodies diluted in TBST (pH 7.4) with 0.1% BSA. The day after, they were rinsed three times with TBST for 3 min each at room temperature and incubated for 1 h at room temperature with peroxidase-labeled secondary antibody diluted in TBST (pH 7.4) with 0.1% BSA. Membranes were washed 6 times, 5 min each, with

TEB is a non-proprietary and specific finding was detected by the national identification system (ICL system (American Biochemicals) using HighSpeed™ (American Biochemicals)).

Primary and secondary antibodies used are: rabbit polyclonal anti-B2C (1:500, n=45), Santa Cruz Biotechnology, Santa Cruz, CA, USA; mouse monoclonal anti-actin (1:1000, MAB316, Sigma). Immunoblot procedure (ECL) using anti-actin secondary antibody (1:10000, American Biochemicals) (Abp) and mouse secondary antibody (1:100000, American Biochemicals).

2.2.6 Western immunoblot assay on C56/BL6J_BDF1

BDF1 spleens were harvested from adult female Wistar-Kyoto, weighing approximately 200 g, cultured and maintained in BDF1's natural habitat F12 (Gibco) for 1 hour under sterile conditions. BDF1 were sacrificed by a lethal ip injection of thiobarbituric acid according with the local Ethics Committee and the European Communities Council Directive 2006/35/EC. Adipose tissues were taken for isolation and dissociation using one or several human adipocytes for culture, cell sorting and cloning. BDF1 spleens were cultured into methylcellulose co-culture (BDF1 Biochemicals) and C56/BL6J_BDF1 for 48 hours and incubated at 37 °C for 1 hour. The medium was filtered (1) in the culture medium. Spleens were incubated for 4 days in culture medium for medium (DMEM) at 37 °C with 10% FCS (2) supplemented with 10 ng/ml rIL-2. After 4 days, spleens were fixed with 4% PFA for 15 minutes at room temperature. For immunofluorescence, briefly, the specimens were incubated overnight in a solution containing both anti-mouse-CD316 (monoclonal mouse 1:200, Sigma), and anti-porcine polyclonal anti-actin (1:1000, Chemicon International) primary antibodies. After washing in PBS, double immunostaining was carried out by incubating sections for 1 h in a solution containing two secondary antibodies: anti-mouse IgG1 (Jackson ImmunoResearch Laboratories) and anti-mouse IgG2A (Pierce and Warriner) (Jackson ImmunoResearch). All samples were observed with a LSM 510

conditioned reflexology system (Elex, Stim), which incorporates two laser diodes and LED's and is equipped with an internal Arduino 101M microcontroller.

2.3 In vitro work on CNGPT20_20P and CNG20P

All procedures were approved by the Scientific Committee of the University of Torino, by the Institutional Animal Care and Use Committee of the University of Torino, and by the Italian Ministry of Health, in accordance with the European Committee Council Directive 2003/63/EEC.

2.3.1 Animals and surgery

In vivo preliminary analysis were performed under general anaesthesia on 2 adult female Wistar rats, weighing approximately 200 g, in order to evaluate behaviour, suitability and the possibility of their use for peripheral nerve injury. Before using C3 microfilament, rats were anaesthetized by 5% isoflurane and placed in a supine position in the range of 10-15 cm. In the first case, the C3 microfilament was used to wrap crushed median nerve and was closed with a suture point (Figure 1 A,B). In the second rat, the C3 microfilament was rolled up and glued with biological cyanoacrylate glue to obtain 1 cm long strands (Figure 1 C,D). Median nerve was transected, 3 mm of median nerve was removed and CNGPT20 and CNGPT20_20P tubes were sutured holding the two nerve stumps (Figure 1 G,H). The two sutured zones made the animals **unable to use affected extremities after surgery**.

Microfilament nerve regeneration analysis were carried out on 10 adult female Wistar rats, weighing approximately 200 g, with transected CNGPT20 and CNGPT20_20P microfilaments, and on 10 adult female Wistar rats, used as controls for untreated nerve stumps.

The animals were divided by three experimental groups of 4 animals each for two groups, the median nerve was transected and repaired with CNGPT20 or CNGPT20_20P constructs. Median nerve repaired with nerve sutured was used as control. The surgical procedure was previously described by Yu and colleagues [21]. The complete and

The animals were adapted during their 4-week retention at the experimental station for each group. In order to prevent interference with the growing test device during testing due to the use of the conventional trough, the conventional medicine were removed at the middle third of the backline and its proximal end was covered in the proximal major area to avoid spontaneous contamination (2). After 12-week post-operative, rats were sacrificed and organometal were analyzed.

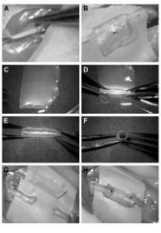


Figure 1. (A) Detail of the main body, (B) (C) main body and in view rotated 90 degrees, (D) (E) (F) main body and in view rotated 180 degrees, (G) (H) main body and in view rotated 270 degrees, (I) (J) main body and in view rotated 360 degrees, (K) (L) main body and in view rotated 45 degrees, (M) (N) main body and in view rotated 135 degrees, (O) (P) main body and in view rotated 225 degrees, (Q) (R) main body and in view rotated 315 degrees.

2.1.2 Fluorescence assessment of chemical markers

Clipping test sections were carried out every 15 weeks until week 12. Clipping test was performed following the same procedure previously described (22) using the BS-Grip Grip Meter (Orthopedic Instruments, Vienna, Italy). The test is carried out by holding the test by the tail and lowering it towards the device and then, when the animal grips the grid (making it descend until it hits its grip). When the marker wears down it is required the animal's paw approaches the grid in a single, rapid extension. The behavior records the maximum weight that the animal manages to hold up before losing the grip. Each animal was tested three times and the average value was recorded. Since assessment of animal welfare was one of the main objectives of the study, a careful daily animal care/behavior was adopted for posture and action measurement, under standardized and quiet conditions, especially during early post-operative times.

2.1.3 Immunohistochemistry and confocal laser microscopy

From all animals, the vertebrae (control, with regenerating discs inside, was three, six and analyzed with immunofluorescence as confocal laser microscopy. Series of 10 µm thick longitudinal sections were cut by a 4 µm-thick vibratome (MT8000, RMC, Tucson, Arizona). Sections were then incubated overnight in a solution containing anti-mouse/mouse IgG2b, primary antibody (conjugated, mouse, which recognizes the 200 kDa subunit of mouse fibronectin, dilution 1:200, Sigma) and then, after washing in PBS, incubated for 1 hour in a solution containing Alexa488-conjugated anti-mouse IgG1 (dilution 1:200, Life technologies). The sections were finally mounted with a Dako fluorescence mounting medium and analyzed by a LSM 1010 confocal laser microscopy system (Bio, Inc, Göttingen).

2.1.4 Discs embedding and electron microscopy

After the 12-week follow-up this material was recombined and the nerve segment fixed in the osmium tetroxide, fixed and prepared for design-based stereological analysis of myelinated nerve fibers and for electron microscopy. Nerve samples were fixed by immersion immersion in 2.5% perfused glutaraldehyde and 0.5% osmium in 0.1 M Tris-cacodylate buffer for 4 h. Specimens were then washed in cacodylate containing 1.5% osmium in 0.1 M Tris-cacodylate buffer, post-fixed in 1% osmium tetroxide, dehydrated and embedded in araldite. From each nerve section of white matter transverse sections (2.5 µm thickness) were cut starting from the distal stump of each myelinated nerve segment using an Ultramicrotome (Leica Microsystems, Wetzlar, Germany) and stained using Trichrome blue for high resolution light microscopy examination and design-based stereology. For transmission electron microscopy ultrathin sections (100-150 nm thick) were cut using the same ultramicrotome and stained with uranyl acetate solution of uranyl acetate and lead citrate. When thin sections were analyzed using a TEM 1000 transmission electron microscope (LEICA, Wetzlar, Germany).

2.1.1. Design-based quantitative morphology of nerve fiber representation

In each nerve segment that contained an LNMP axon, design-based stereological analysis was applied and using our randomly selected arbitrary thin section method section. A DM6000B microscope equipped with a DIC/DM digital camera and an SEMV image manager system (Leica Microsystems, Wetzlar, Germany) was used for stereology. The final magnification was 5000X enabling us to see myelinated and unmyelinated axons of myelinated nerve fibers. From each thin section from each nerve was randomly selected and the total cross-sectional area of the nerve was measured. The sample of fibers in each nerve was then randomly selected using a previously described stereological method [25]. Two-dimensional diameter profiles were also used to which an additional representative sample of myelinated nerve fibers. Fiber number was calculated from fiber and area [6].

data were measured and the risk being measured of their (2) and none of them calculated. These data were used to calculate specific likelihood (3)–(5), and the prior (24).

2.4 Methods

For in vitro experiments, data were reported as mean \pm SEM. Statistical analysis was carried out using single-factor analysis of variance (ANOVA) post hoc Bonferroni. Values of * p < 0.05, ** p < 0.01, *** p < 0.001 were considered as statistically significant. For in vivo experiments data were reported as mean \pm SD. Statistical analysis was carried out using Two-sample t -Test. Values of * p < 0.05, ** p < 0.01, *** p < 0.001.

3. Results

3.1 In vitro cell based on C5 based samples

3.1.1 Cytotoxicity study on C5GFP26, GFP and C5GFP

The effect of the C5 based material on cells was evaluated by RTG-2 (RTG) proliferation assay counting the number of proliferating cells after 2, 5, 7, 9 and 10 days (Table 1). RTG-2RT showed the lowest of C5GFP and C5GFP26, GFP showed no cytotoxic effect since no significant differences in cell number were detected between these two culture conditions and the control.

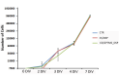


Figure 2. Evaluation of the effect of incubation period on the adhesion of R19-DRIFT cells to CS-GP130 and CS-GP130-DSP substrates.

1.1.2 Cell adhesion on CS-GP130-DSP substrates

R19-DRIFT cells were seeded on CS-GP130-DSP and on control glass-immunocytochemistry medium was performed after 24 hours of culture to specifically evaluate cell adhesion and morphology. In order to obtain a more detailed evaluation of cell adhesion, the cells cytoskeleton and focal adhesion complex were stained using TRITC-conjugated phalloidin and anti-beta-actin antibody, respectively. R19-DRIFT cells internalized and compared with CS-GP130-DSP substrates. Differences in morphology and size were observed when R19-DRIFT cells were cultured on control glass and CS-GP130-DSP (Figure 3). Cells on control glass displayed a higher rate, they were also more spread without particular orientation of the actin cytoskeleton (Figure 3A and C). Cells cultured on CS-GP130-DSP displayed a more elongated morphology characterized by a typical head-tail cell body with long protrusions, giving an overall spindle shape that is typical of ECs (Figure 3B and 3D).

The analysis of the morphology of these cells placed on different substrates showed that the cells of cells placed on control substrates (glass) presented a flattened form, similarly to fibroblasts, and only

DN as depicted above relative to SC. By contrast, 50% of the cells cultured on CSOPDM_2MP had generated the SC-like elongated shape.

Viability immunostaining was performed to visualize the exact location of focal adhesion sites.

Viability-positive sites were observed on cells seeded both on control and CSOPDM_2MP, but with different distributions. CSOPDM_2MP membranes presented cells with a higher concentration of viabilities around the tracks (Figure 3F) while protein concentrations at the edges of cells was slightly elevated in control (Figure 3G).

3.3.3. Proliferation assay on CSOPDM_2MP membranes

Proliferation assay was performed on CSOPDM_2MP samples (Figure 3G). R3-2D4ST2 cells were cultured on both CSOPDM_2MP and glass plates (control). The number of proliferating cells was determined after 7 days (DN).

R3-2D4ST2 cells seeded on CSOPDM_2MP showed lower proliferation rates and significant differences in cell numbers were detected in the culture conditions after 7 DIV (**p<0.01) and 4 DIV (***)p<0.001), in comparison to positive control. Yet, it was possible to observe a constant increase of cell numbers on CSOPDM_2MP samples at each time point.

3.3.4. Gene and protein expression of *WNT4* and *WNT5A* cultured on CSOPDM_2MP samples

Both *WNT4* and *WNT5A* mRNA expression changes were evaluated to study progenitor and cell survival signaling after 7 and 4 days of culture of R3-2D4ST2 cells on CSOPDM_2MP samples.

The relative values of *WNT4* and *WNT5A* mRNA expression were not significantly different when comparing CSOPDM_2MP with control conditions, both after 7 and 4 days of culture. (Data not shown). By contrast, significant differences in the *WNT5A* mRNA expression was observed after 7 days of

which T_H17s respond to the context although the difference was not observed after 6 days (Figure 1B).

The same pattern of expression was detected at the protein level. The decreased protein expression of IL-17 after three days of culture of the WT-DMP12 cells on thymus medullators, undergoes a clear recovery after six days of culture, although not to the measured values (Figure 1C).

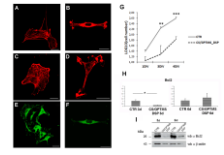


Figure 1. Cell surface expression of cytokines. (A) Intracellular expression of IL-17 in WT-DMP12 cells cultured on thymus medullators for 3, 6, and 9 days. (B) IL-17 mRNA levels in WT-DMP12 cells cultured on thymus medullators for 3, 6, and 9 days. (C) IL-17 protein levels in WT-DMP12 cells cultured on thymus medullators for 3, 6, and 9 days. (D) IL-17 protein levels in WT-DMP12 cells cultured on thymus medullators for 3, 6, and 9 days. Error bars represent standard deviation. *p < 0.05, **p < 0.01, ***p < 0.001.

3.1.1. Media and growth media for CSOPFNs_DSP

DMEM medium was purchased from Gibco. Media was used and cultured for 4 days on uncoated control coverslips and CSOPFNs_DSP for neurite outgrowth. The cultures were fixed and immunostained for NF-200. Media present and peripheral axons and their contact with basal laminar membrane. A double labeling immunofluorescence revealed that both neuronal differentiation. Neurite proteins were expressed by DMEM neurons (Figure 6).

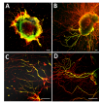


Figure 6. The immunofluorescence images of neural outgrowth of 4 days after PBN culture medium on uncoated control coverslip (a, c) and CSOPFNs_DSP for neurite outgrowth (b, d). Yellow color indicates co-localization of the two markers.

3.2. In vitro performance analysis

In order to evaluate neurotoxicity for peripheral nerve injury, the neurotoxicity of CSOPFN and CSOPFNs_DSP were tested in vitro in adult female Wistar rats.

Both neurotoxicity tests in the laboratory of PBN were used to make these tests. Diagram can help size and shape of neurotoxicity depending on the size of the nerve and the lesion type and extent. They can be used to predict an injured nerve from adhesion (Figure 7B) or as a model to help a nerve defect (Figure 7C). Both neurotoxicity methods to help a good neurotoxicity after the PBN immersion.

and the recovery time was significantly smaller in patients in the operation site, and they are easily related to the fact that CSOPMS, DSP methods by much more light.

3.3 In vitro tests with CSOPMS, DSP and CSOPMS, DSP and CSOPMS, DSP

3.3.1 Postoperative assessment of functional recovery

In vivo nerve regeneration experiments were carried out with both CSOPMS and CSOPMS, DSP methods. The maximal motor recovery of female Wistar rats was evaluated by raised up and side-lap CSOPMS or CSOPMS, DSP methods. Behavioral analysis were performed (analogous report was used as control).

Figure 5 reports the post-operative time course of functional recovery for rats treated using CSOPMS and CSOPMS, DSP. In the group of CSOPMS, DSP methods, functional recovery of finger flexor muscle EMG increased during of post-operative period. This observed to be due to the detection of CSOPMS, DSP after time for distal nerve repair.

The function of finger flexor muscle, measured by the median nerve tested to recover faster for animals receiving a performance remarkably different from CSOPMS at week 4 after lesion ($p < 0.05$). Functional recovery in CSOPMS showed at week 4 and progressively increased. At week 8 and 12, no more significant differences were detectable between original and CSOPMS treatment.

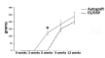


Figure 5. Post-operative assessment of functional recovery. Line graph showing the post-operative time course of functional recovery in animals in the groups CSOPMS (solid line) and CSOPMS, DSP (dashed line). Significant differences between CSOPMS and CSOPMS, DSP recovery were observed at weeks 4, 8 and 12 ($p < 0.05$).

3.2.2 Immunohistochemistry and confocal laser microscopy

Axonal regeneration was analyzed by confocal laser microscopy on longitudinal nerve lesion sections after immunohistochemistry staining (Figure 6). After 12 weeks post injury, the axonal sprouts of both C5GPR56, GFP and C5GPR56, GFP control indicated SP axons regrowing from lesion, with distal axonal and synaptic varicosities in the C5GPR56, GFP control (Figure 6A) and finally axonal in C5GPR56 control (Figure 6B).



Figure 6. *In vivo* axonal sprout evaluation. Transverse sections on longitudinal sections of 12 weeks control and C5GPR56 and C5GPR56, GFP were paraffin embedded and were C5GPR56, GFP and GFP stained. Axonal sprouts were seen both proximally (control and C5GPR56, GFP) while properly formed axonal SP axons were found in C5GPR56, GFP and GFP.

3.2.3 Light and transmission electron microscope analysis

Figure 7 shows high-resolution light and transmission electron microscope images of the distal rat median nerve injured, repaired with sutured or C5GPR56 control and harvested at 12 weeks post operation. Distal median nerve treated with C5GPR56, GFP was an increased lesion area, axonal sprouts were detected from the distal sutured site. Small myelinated axons and microvilli-like filopodia of regenerated axons were detected both on nerves sutured with sutured (Figure 7 A,C,E,G) and with C5GPR56 control (Figure 7B,D,F,H).

Maximal transduction efficiency observed when used with 2000 in early stages of myelination (Figure 7E,F) as well as myelinated fibers (Figure 7G,H), in axons before myelin sheath with CS-DSP coated and silk-coated.

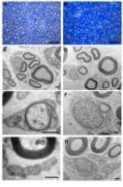


Figure 7. Myelinated axons. Presence of axons in myelinated fibers is represented in the top row of electron microscopy images (middle and bottom rows). (A) CS-DSP coated, (B) silk-coated, (C) CS-DSP coated, (D) silk-coated, (E) CS-DSP coated, (F) silk-coated, (G) CS-DSP coated, (H) silk-coated. Scale bars: (A) 200 nm, (B) 200 nm, (C) 200 nm, (D) 200 nm, (E) 200 nm, (F) 200 nm, (G) 200 nm, (H) 200 nm.

2.2.3. Single-blind, parallel, randomized controlled trial of acute pain management
 12-week post-operative, single-blind, randomized trial of regional analgesia versus regional with CSFOP sites or control (sham) needles in terms of total number of analgesic doses (range 0-10) (CSFOP = 5000). Anal and then diameters and Gracis are significantly lower (p<0.05) in patients versus regional with CSFOP sites when compared to analgesic, while morphine has been shown to require less (p<0.05).

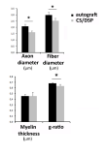


Figure 4. Mechanism of action of regional analgesia. For single-blind, randomized controlled trial of acute pain management versus regional with CSFOP sites or control (sham) needles in terms of total number of analgesic doses (range 0-10) (CSFOP = 5000). Anal and then diameters and Gracis are significantly lower (p<0.05) in patients versus regional with CSFOP sites when compared to analgesic, while morphine has been shown to require less (p<0.05).

4. Discussion

Application of CS to bone engineering is a very novel and exciting topic [13,23]. This biomimetic structure not only for the high biocompatibility and biodegradability, but also for the anisotropic properties and the absence of immune responses.

However, physical and mechanical properties of CS when it is associated with various solutions have to be carefully considered in order to apply it properly for regenerative purposes.

In the manuscript CS was treated with crosslinking agents able to act on its chemical, physical and mechanical properties, mainly γ -polyvinylpyrrolidone (PVP), ethane sulfonic phosphonate (ESP) and a combination of PVP and ESP (PVP+ESP), as previously described by Birkedal colleagues [25].

The present of PVP and ESP allowed that these agent was homogeneously distributed in the developed hydrogels and increased the water stability and the stiffness of CS/PVP, ESP and PVP+ESP.

Stiffness of CS/PVP hydrogels

Both CS/PVP+ESP and CS/ESP the membranes were studied *in vitro* and *in vivo* for the implementation of CS-based nerve scaffolds.

First of all, the presence of degradation of the CS membranes, both CS/ESP and CS/PVP+ESP, showed no major effects on physical and mechanical properties.

Yet, preliminary analysis of glial cells number in CS/PVP+ESP membranes led to confirm that CS is capable to support glial cell proliferation [25] although delayed in comparison to previous studies.

This is attributable to the need for an initial adjustment in the new culture. The need of adjustment of the cells in the culture was demonstrated also by gene expression analysis of the cell progeny phase.

In CE that is significantly lower in the genes for 3 days on CS/PVP+ESP while the difference was no more detectable after 6 days.

The results of cell cultures in the C3GFPMS_DBP conditions showed that glial cells exhibited a different morphology and actin and tubulin distribution, supporting the view that they rely on a higher migration capacity on the basement, a key requirement for the early stages of nerve regeneration [24]. The actin cytoskeleton is a highly dynamic network composed of actin polymer and a large variety of associated proteins. The function of the actin cytoskeleton is to maintain variety of essential biological functions, including intracellular and extracellular movement and structural support. The orientation and distribution of actin filaments within a cell is, therefore, an important determinant of cellular shape, adhesion and motility [25].

The movement of the membrane of neurons with the neuronal cytoskeleton is a key pre-requisite step in evolution, in vitro, the potential for neural regeneration. Exponent of neuronal morphology (ENMG) is a valuable *in vitro* model to observe the neurite outgrowth in different substrates [26]. In our research, while ENMG was cultured on C3GFPMS_DBP substrates and on glass, in control. After four days a high number of neurites sprouting from each of the control and control plates, was observed, on both substrates. Although quantitative analysis was not conducted, careful observation led to detect a greater spreading and neurite extension on the C3 substrate in comparison to control.

In preparation of *in vitro* experiments, a series of preliminary work allowed us to evaluate the permeability of C3 membranes. It was possible to establish the very binding and the possibility to build at the time of the surgery a tube of specific size and shape depending on the nature of nerve damage, although it was evident that the C3GFPMS_DBP is much more flexible in comparison with C3 itself.

Both C3GFP and C3GFPMS_DBP conditions were used for bridging across 10 mm long rat median nerve defects, and the outcome of 12 weeks post-implantation was evaluated by functional, immunohistochemical and histological investigations. We observed that C3GFPMS_DBP shows some attached from the dorsal sensory root, due to excessive flexibility, and then an functional recovery [27].

conductor. This result was confirmed by confocal laser microscopy which displayed very poor axonal representation with an irregular orientation inside Cx36/PTSD₁ PSD conductors.

By contrast, Cx36/PTSD₁ showed functional recovery that started at week 4 and progressively increased reaching values similar to untreated already at week 6. The delayed functional recovery is justified by the different repair techniques used in line with the results obtained using other types of conductors [24].

Interestingly, morphological analysis showed distinct subtypes typical of regenerated nerve fibers with small nerve fibers at different regeneration stages and myelinated fibers. Though morphological analysis revealed that Cx36/PTSD₁ has, on average, smaller fibers than untreated.

F. Conclusions

In this work, we have evaluated a histological quality control battery of rat conductors for axonal representation, biodegradability, axonal conductivity, and axonal growth activity. Considering different bio-printed channels we will optimize mechanical properties for successful application in the field of peripheral nerve regeneration.

Our experiments showed that Cx36/PTSD₁ results promote peripheral nerve regeneration with an outcome close to that reached by nerve autografts which are generally considered as the gold standard for treating severe nerve defects. These newly developed nerve guides should thus be regarded as promising alternatives to traditional nerve autografts.

However, it could be interesting to combine our channel conductors with filling materials composed with growth factors [24] which are able to further increase the effectiveness of the scaffold device. Yet, creation of a 3D inner structure, which simulates extracellular matrix, might also provide a further support to axon and glial cells [21,22,23]. Therefore, although the device that we propose is simple

and any further changes. Some requirements should clearly indicate the functional behavior of the considered software when the further increase the operation period of the device.

Acknowledgments

The research was supported by Regione Piemonte - PIA di Innovazione - INCOGNITE project number 190/2017.
The authors declare no conflict of interest.

References

1. Dai, W., Yan, Y., Ding, D., Wu, B., A. Patel, A. (2011) A hierarchical approach to peripheral neuropathic pain relief by peripheral nerve gap and continuous electrical current. *J. Neurosci.* 31: 1511-1520.
2. Grewal, A., Lurie, A., Pappas, M., Fawcett, J., Turner, D., et al. (2003) Effect of genetically modified Schwann cells with increased myelin on peripheral nerve grafting. *Neuroreport* 14: 427-432.
3. Li, F., Wang, X., Gao, Y., Wang, A., Wang, M. (2004) Transfection of peripheral nerves, bridging nerve gap after transection. *Neurosci Lett* 361: 159-162.
4. Katsuno, S., Fukuoka, M., Tan, F., Ruitman, R., Gao, Y., et al. (2011) Perspectives in regenerative medicine: engineering of peripheral nerve with stem cell. *Cell* 145: 104-116.
5. He, H., He, T., Tang, H., et al. (2012) Nonparacrine signal and gene transfer efficiency for MSCs on cultured and Schwann cell-based peripheral nerve. *Neurosci Lett* 425: 203-207.
6. Mochly, A., Elgarni, A., Mochly-Rosen, M., Mousavi, A., Mousavi, R.A. (2013) Schwann cell-like genetic control and Schwann cell-like differentiation of neural stem cells. *Neurosci Lett* 454: 101-105.
7. Yan, X., Zhang, H., Song, Y., Wang, X., Gu, X. (2011) The interaction of Schwann cells with cultured neuroblastoma cells *in vitro*. *Neurosci Lett* 497: 427-430.
8. Datta, S., Kulkarni, R., Kulkarni, K., Shukla, M. (2005) Correlation of adhesion and degradation of Schwann cells by neurotrophic factor. *Neurosci Lett* 385: 157-160.
9. Sano, M., Goto, A., Shimizu, Y., et al. (2011) Schwann cell-derived exosomes and their role in vivo Schwann cell maturation during peripheral nerve regeneration. *Neurosci Lett* 491: 141-145.
10. Gao, Y., Wang, X., Wang, X., et al. (2011) Schwann cell-derived exosomes and their role in vivo Schwann cell maturation during peripheral nerve regeneration. *Neurosci Lett* 491: 141-145.
11. Gao, Y., Wang, X., Wang, X., et al. (2011) Schwann cell-derived exosomes and their role in vivo Schwann cell maturation during peripheral nerve regeneration. *Neurosci Lett* 491: 141-145.
12. He, H., He, T., Tang, H., et al. (2012) Nonparacrine signal and gene transfer efficiency for MSCs on cultured and Schwann cell-based peripheral nerve. *Neurosci Lett* 425: 203-207.
13. Mochly, A., Elgarni, A., Mochly-Rosen, M., Mousavi, A., Mousavi, R.A. (2013) Schwann cell-like genetic control and Schwann cell-like differentiation of neural stem cells. *Neurosci Lett* 454: 101-105.
14. Yan, X., Zhang, H., Song, Y., Wang, X., Gu, X. (2011) The interaction of Schwann cells with cultured neuroblastoma cells *in vitro*. *Neurosci Lett* 497: 427-430.
15. Datta, S., Kulkarni, R., Kulkarni, K., Shukla, M. (2005) Correlation of adhesion and degradation of Schwann cells by neurotrophic factor. *Neurosci Lett* 385: 157-160.
16. Sano, M., Goto, A., Shimizu, Y., et al. (2011) Schwann cell-derived exosomes and their role in vivo Schwann cell maturation during peripheral nerve regeneration. *Neurosci Lett* 491: 141-145.
17. Gao, Y., Wang, X., Wang, X., et al. (2011) Schwann cell-derived exosomes and their role in vivo Schwann cell maturation during peripheral nerve regeneration. *Neurosci Lett* 491: 141-145.
18. He, H., He, T., Tang, H., et al. (2012) Nonparacrine signal and gene transfer efficiency for MSCs on cultured and Schwann cell-based peripheral nerve. *Neurosci Lett* 425: 203-207.
19. Mochly, A., Elgarni, A., Mochly-Rosen, M., Mousavi, A., Mousavi, R.A. (2013) Schwann cell-like genetic control and Schwann cell-like differentiation of neural stem cells. *Neurosci Lett* 454: 101-105.
20. Yan, X., Zhang, H., Song, Y., Wang, X., Gu, X. (2011) The interaction of Schwann cells with cultured neuroblastoma cells *in vitro*. *Neurosci Lett* 497: 427-430.
21. Datta, S., Kulkarni, R., Kulkarni, K., Shukla, M. (2005) Correlation of adhesion and degradation of Schwann cells by neurotrophic factor. *Neurosci Lett* 385: 157-160.
22. Sano, M., Goto, A., Shimizu, Y., et al. (2011) Schwann cell-derived exosomes and their role in vivo Schwann cell maturation during peripheral nerve regeneration. *Neurosci Lett* 491: 141-145.
23. Gao, Y., Wang, X., Wang, X., et al. (2011) Schwann cell-derived exosomes and their role in vivo Schwann cell maturation during peripheral nerve regeneration. *Neurosci Lett* 491: 141-145.
24. He, H., He, T., Tang, H., et al. (2012) Nonparacrine signal and gene transfer efficiency for MSCs on cultured and Schwann cell-based peripheral nerve. *Neurosci Lett* 425: 203-207.

15. Cheng SH, Deng J, Tang F, Cheng Y, Zhou X, et al. (2015) Dual cylindrical propylene and acrylonitrile copolymer film from lithium and gelatin solutions. *Macromolecules* 48: 2017–2024.
16. Wang M, Hu W, Cao Y, Liu Y, Wu J, et al. (2015) Dual ionic-ionic supercapacitors across a 3D porous scaffold by carbonized MOF with calcium gel. *Chem Mater* 27: 1071–1078.
17. Wang M, Xu Q, Wu Y, Gong M, Liu X, et al. (2015) Physical properties and biocompatibility of porous polyurethane foam for supercapacitor storage for nerve regeneration. *Biomaterial* 74: 20–28.
18. Yang X, Gu X, Liu M, Hu W, Wang X, et al. (2016) Fabrication and properties of a porous polyurethane scaffold for nerve regeneration. *Biomaterial* 74: 1711–1721.
19. An Q, Jiang YK, Tian HJ, Guo J, Zhu BC, et al. (2015) The regeneration of neuronal axonal sprouts of rat sciatic nerve injured with four months chronic axotomy. *Neuroscience* 310: 76–86.
20. Xiao F, Xiao F, Tang C, Chen X, Guo H, et al. (2015) Chemical modification for tissue engineering applications of polyurethane scaffolds. *Biomaterial* 70: 100–108.
21. Gu F, Zhou H, G. Nicholas S, Andrian C, Karamali A, et al. (2016) Enhancement of the tissue ingrowth inside for the peripheral regeneration of peripheral nerve regeneration. *J Neurosci Methods* 269: 109–127.
22. Gu F, Zhou H, G. Nicholas S, Andrian C, Karamali A, et al. (2016) Chapter 4 Methods and protocols in peripheral nerve regeneration: A systematic review. *Int J Neurosci* 126: 103–116.
23. Andrian C, Guo H, Zhou H, Guo H, et al. (2016) Evaluation of the neurotrophic activities of the sprouts of myelinated axons in the rat sciatic nerve: a preliminary study. *J Neurosci Methods* 267: 94–100.
24. Naranjo GS, Page SM, Vetterlin L, Barone M, Barone D. (2010) Chondroitinase based up-collagen and laminin 512 porous bone tissue engineering. *Acta Mater* 58: 3467–3474.
25. Li Q, Zhou X, Zhou W, Zhang L, Wang C, et al. (2014) Porous chitosan scaffolds with surface microporosity and inner porosity and their effect on Schwann cells. *Biomaterial* 35: 4151–4161.
26. Chen YH, McEwen DJ, Cheng C, Mognetti B, Russell J, et al. (2015) Axon and Schwann cell permeability during nerve growth. *Development* 142: 1421–1432.
27. Johnson ME, Kopp MB, Andrian C, Berry DS, Bao H, et al. (2015) F-actin bundles affect the survival of neurons in a peripheral nerve through cell-to-cell signaling. *J Cell Biol* 198: 1011–1021.
28. Zhou X, Karamali A, Fagnano J, Shavari, Ezzik, K, Gorke C. (2016) In vivo models for peripheral nerve regeneration. *Dev Neurosci* 61: 207–216.
29. Goshwami G, Patel D, Bhandal G, Mishra M, Singh SB, et al. (2015) Axonal density of the "Nerveless" regenerating peripheral nerve (RN) has a positive effect on regenerated nerve fiber maturation. *Cell Tissue Res* 22: 961–967.

20. Mangan, M., Winkler, S., Nagendran, P., Zhu, H., Wang, C., Shihata, A., et al. (2014) Neurobiology versus neuroengineering: an emerging paradigm in the convergence of neural data and theory. *Int. J. Neurosci.* 24, 1-10.
21. Green, S., Green, S., Proctor, S., De, P., Buitrago, M. (2013) From engineering and peripheral nerve regeneration to neuroscience. *Int. J. Neurosci.* 23(1), 1-11.
22. Green, S., Proctor, S., Buitrago, M., De, P., Wang, C., Wang, C., et al. The influence of electrospun scaffolds on the behavior of peripheral nerve and axonal regeneration. *Appl. Sci. Technol. Chem. Res.* 4(1), 1-10.
23. In, R., Lee, C., Hwang, M., Kim, S., Kim, S., Kim, S., et al. (2009) Designing ideal scaffold for peripheral nerve repair. *Neurosci. Biomed. Res.* 36, 1-10.